TOPOGRAPHIC SURVEY OF AN OPEN CHANNEL IN A TIDAL FLAT

Yen-Chang Chen
Department of Civil Engineering, National Taipei University of Technology, Taipei, Taiwan, R.O.C.

Sheng-Hsiung Hung
Department of Soil and Water Conservation, Taichung, Taiwan, R.O.C

Yi-Jiun Liao
Department of Civil Engineering, National Taipei University of Technology, Taipei, Taiwan, R.O.C

Wei-Po Huang
Department of Harbor and River Engineering, National Taiwan Ocean Engineering, Keelung, Taiwan, R.O.C.

TOPOGRAPHIC SURVEY OF AN OPEN CHANNEL IN A TIDAL FLAT

Acknowledgements

TOPOGRAPHIC SURVEY OF AN OPEN CHANNEL IN A TIDAL FLAT

Yen-Chang Chen[1], Sheng-Hsiung Hung[2], Yi-Jiun Liao[3], and Wei-Po Huang[4]

Key words: bathymetry, open channel, topographic survey, tidal flat.

ABSTRACT

This paper describes the fundamental characteristics of an open channel in a tidal flat. In this study, the open channel was characterized using a topographic survey. Because of the limited resources available and special measurement conditions at the study area, cranes and cables were used to transport a sounding weight to the measurement point, and pressure gauges hanging on the sounding weight were used to measure the water depth. The coordinates and altitude of the surface point above the sound weight were measured using a total station. The kriging interpolation was applied to discrete geographic data to create contour lines and a topographic map of the open channel in the tidal flat. This methodology is simple, accurate, and cost-effective. Therefore, the developed methodology and theory can be applied to bathymetry measurements of river terrains with similar conditions.

I. INTRODUCTION

Open channels in tidal flats are characterized by oscillating currents and bathymetries dominated by two periodic cycles (Chen et al., 2013), namely the semidiurnal tide cycle and the spring and neap tide cycles (Garrison, 2007). A semidiurnal tidal cycle comprises two nearly equal high tides and low tides every lunar day and has a period of 12 hours and 25 minutes. It theoretically has a wavelength of more than half the circumference of the Earth (Schwiderski, 1980). Spring tides occur at new moon and full moon, and neap tides occur during the first and third quarters of the moon. Thus, these tides occur twice each lunar month, and the spring/neap cycle is 29.52 days (Kvale, 2006). Because every
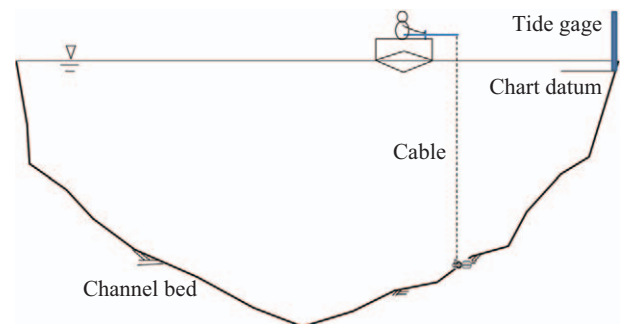
Fig. 1. Conventional depth measurement method.

tidal channel has a unique orography, considering the bathymetric variation during topographic surveying is critical. Manual techniques for bathymetry measurement include the usage of hand cables, topographic level rods, and sounding poles. Conventional sounding is usually performed mechanically; bathymetry is measured using a rigid sounding pole or a sounding weight suspended from a cable. As illustrated in Fig. 1, the sounding weight is suspended in water by a cable from a boat. When the weight hits the bottom of the channel, the line becomes slack. The weight is then pulled back up, and the distance from the channel bed to the water surface is measured. The conventional method is simple but labor intensive and costly. Generally, the manual method is used where efficient acoustic methods cannot provide adequate depth data or sufficient detail (US Army Corps of Engineers, 2004). The application of sonar changed the method for measuring bathymetry. A variety of sonar systems, such as single beam transducer systems (Rantz, 1982; Gupta et al., 2012), multiple transducer channel sweep systems (Pacheco et al., 2010), and multibeam sweep systems (Clarke et al., 1996), are used depending on the measuring conditions and depth. Sonar systems measure the time taken by an acoustic pulse to travel from a generating transducer to the channel bottom and back to the transducer. Therefore, the depth can be computed by multiplying half the travel time of the pulse and the velocity of sound in water. Recently, systems comprising a global positioning system (GPS) and airborne laser bathymetry have been used to measure the depth in shallow water (Wang and Philpot, 2007; Pe'eri et al., 2011). Compared with multibeam sweep systems, the swath width of sonar systems decreases with decreasing depth. Airborne lidar bathymetry is an efficient remote sensing
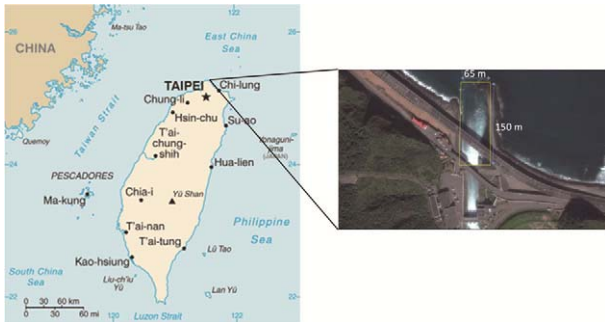
Fig. 2. Location of the study area in Taiwan.

Fig. 3. Flow conditions in the open channel.

technique for shallow water mapping. Most lidar systems employ two spectral bands; one detects the water surface and the other detects the water bottom. The depth of the water is determined from the difference between the travel times of laser pulses reflected from the surface and bottom. However, the depth, water clarity, composition and type of bottom material, eye safety, weather, state of the sea, and background light, influence the surveyable depth (Muirhead and Cracknell, 1986). Usually, the surveyable depth is between 2 and 3 times the Secchi depth (Guenther et al., 2000).

These sophisticated topographic survey methods were difficult to apply in the study area. Therefore, a simple and reliable method was developed for measuring the bathymetry of the channel, which met the most critical requirement for accurate depth measurements. Bathymetric contours were plotted for the channel according to the kriging method.

II. STUDY SITE DESCRIPTION

Fig. 2 displays the location and aerial photograph of the estuary in the A-Li-Bon creek. A 150-m-long and 60-m-wide section of the channel was selected for the topographic survey. The channel is an artificially regulated river with concrete embankments and armor blocks for preventing wave damage.

The A-Li-Bon creek is located in northern Taiwan and has a length of 12.10 km with a drainage area of 10.03 km^2, which is distributed throughout His-Men District of New Taipei City. The creek originates at an altitude of 1,074 m at the northern end of Yangmingshan National Park's Zuzi peak. Abundant with water, its main stream meanders from south to north before emptying into the East China Sea at the eastern side of the Shi Ba Wang Gong (Eighteen Lords) Temple at Taiwan's northernmost end. Geologically, the northern coast of Taiwan is formed by waves and tides, which results in sea erosion and sedimentary topography. Therefore, the study area featured a rocky seabed. According to statistics from the observatory at Caoli Fishing Port, which is close to the study site, the highest observed tide was 1.65 m and the lowest was -1.47 m. The mean high and low waters were 0.61 and -0.52 m, respectively. The monsoon tides in the winter had a height of 0.8-5.2 m and a cycle of 5-9 seconds. The highest wave had a height of 5.2 m with a cycle of 9.4 seconds. Considering the recurrence of typhoon waves for 50

years, the northeastward wave from the typhoon waves hitting the study area had an estimated height of 10.91 m.

According to observations from 2009 to 2016, the rainfall near the tidal flat was 1,285-2,272 mm with an annual average of 1881.8 mm. The A-Li-Bon creek has a short length but significant drop heights, resulting in strong currents with a velocity of up to 5 m/s near the tidal flat. This prevents hydrologists from measuring the terrain by wading through the water. The flow conditions at the estuary of the open channel are displayed in Fig. 3. Strong currents and drastic changes in depth prevent boats from approaching the channel. Therefore, measuring the depth using conventional methods is impossible. Furthermore, bubbles form from the rugged terrain preventing the application of a sonar system in the area. In addition, airborne lidar bathymetry is unsuitable because of the increased opacity caused by bubbles and strong currents.

III. METHODOLOGY

Data quality, depth measurement accuracy, capability, and cost-effectiveness were the primary considerations in the design, construction, and operation of the proposed bathymetry measurement system. Because of the limited demand and difficulty in meeting the conditions of the study area, the proposed topographic survey method involved a bathymetry measurement system and kriging interpolation.

1. Bathymetry Measurement System

Considering the limitations of the study area, a pressure gauge was used for measuring the bathymetry. Two identical pressure gauges were attached to both sides of a sounding weight, which was sunk to the bottom of the channel. The average readings from the two pressure gauges were used to estimate the water depth.

The bathymetry measurement system comprised a theodolite, three cranes (each mounting bracket included a hoisting apparatus and fixed pulley), cables, diverting pulleys, reflective prisms, buoys, a sounding weight, and three pressure gauges, as displayed in Fig. 4(a). The crane, cables, and pulleys were mainly used to
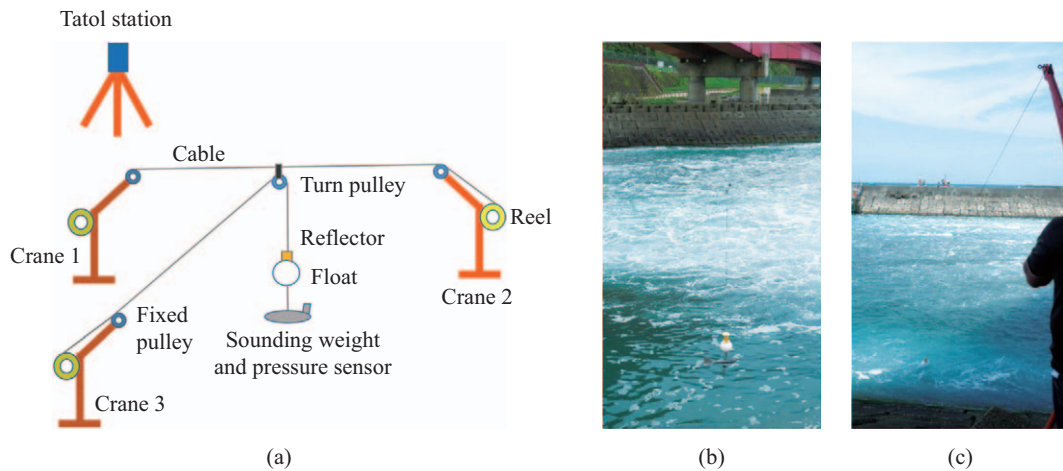
Fig. 4. Bathymetry measurement system; (a) scheme of the hardware setup for measuring the bathymetry; (b) reflector, float, sounding weight, and pressure sensors; and (c) transfer of the sensors to the desired measurement locations using cranes.

control the positions of the pressure gauges. The buoys were used to maintain the reflective prisms above the water surface. The sounding weight was used to sink pressure gauges to the bottom of channel bed. Because the tidal stream was swift, a Columbus 50-lb sounding weight streamlined to offer minimum resistance to the flowing water was used to maintain the pressure gauge stationary in the water. Thus, pressure gauges could be installed at the desired locations.

During measurement, cranes 1 and 2 were used to transport the pressure gauges to the measurement points by adjusting the pulley through winding and rewinding. Subsequently, crane 3 was used to manipulate the movement of the Columbus-type weight and pressure gauges. The cables attached to the sounding weight and pressure gauges could pass through the holes in the center of the buoys and reflective prisms. The operators of crane 3 straightened the cable (Fig. 4(c)) when the sounding weight sunk to the bottom (Fig. 4(b)). This caused the buoys and prisms to float on the surface above the sounding weight. The operator of the total station located at the onshore reference point read out the Cartesian coordinates of the prism and average water surface elevation. To prevent data loss caused by malfunction of the pressure gauge, two identical pressure gauges were attached to both sides of the sounding weight.

Ideally, the buoys float directly above the sounding weight when it sinks to the riverbed. However, the buoys were marginally deviated by the water currents. Two steps were applied to reduce this deviation: (1) The cable was marginally rewound to tighten it after the sounding weight touched the channel bed, which prevented the buoys from flowing downstream; and (2) the diverting pulleys, buoys, and sounding weight were maintained as close as possible to the water surface at the torrential areas. Subsequently, the sounding weight was marginally immersed to determine the Cartesian coordinates. Next, the sounding weight was sunk rapidly to the channel bed to determine the depth. When the sounding weight was suspended in water, it

drifted because of the swiftly flowing water as well as the measured pressure varying with time. Unstable pressure readings indicated that the sounding weight and pressure gauges were suspended in water and did not touch the bottom of the channel. Generally, the waves in the studied tidal channel were ripples and their magnitude exhibited only small variations. Therefore, the pressure variation caused by the waves was small compared with the atmospheric pressure. If the pressure gauges lay on the channel bed, the changes in pressure and time were represented by a steady horizontal line, as displayed in Fig. 5(b). In areas with sluggish flow, the cables could be straightened when the sounding weight touched the channel bottom, which allowed the buoy to be directly above the sounding weight. The sounding weight and buoy were affected by torrents. The two situations observed during the implementation are described as follows. During high tide, the water flowed upstream to offset a part of the drainage and reduced the velocity, which made it possible to straighten the cable when the sounding weight touched the channel bottom. Therefore, the buoy was mostly above the sounding weight. During low tide, the water flowed into the sea with a high speed and the sounding weight and buoys marginally drifted downstream. Here, the diverting pulleys, buoys, and the sounding weight were maintained as close as possible to the water surface in the torrential areas. Subsequently, the sounding weight was marginally immersed to determine the Cartesian coordinates. Next, the sounding weight was rapidly sunk into the water to determine the water depth. The water was shallow during the ebbing tide, which resulted in low errors caused by the deviated cables.

2. Kriging Interpolation

After the survey data of the channel bottom were obtained, kriging interpolation was used to produce contours. The kriging technique is also known as the geostatistics technique. Kriging interpolation is used to determine the linear interpolation factor
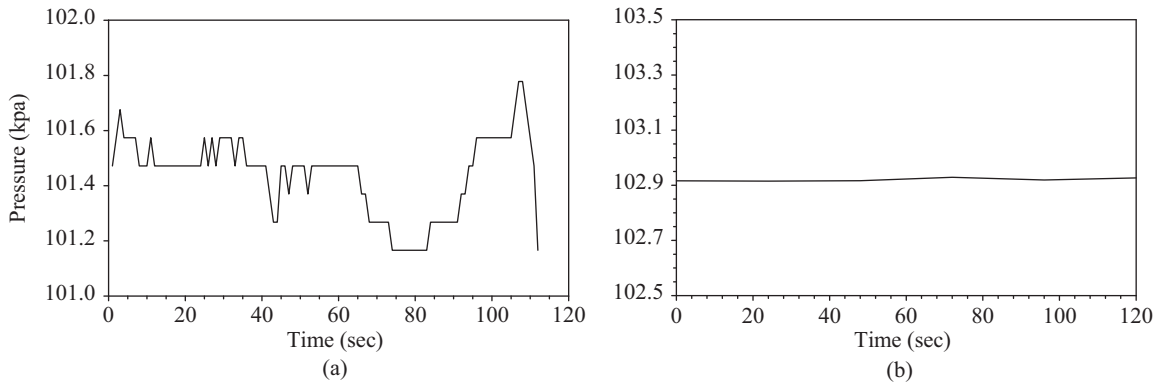
Fig. 5. Pressure variations; (a) sounding weight and pressure gauge suspended in water; and (b) sounding weight and pressure gauge resting on the bottom of the channel.

according to the statistical characteristics of spatially distributed data (Rodriguez-Iturbe, 1982). Three main kriging methods exist, namely simple kriging, ordinary kriging, and universal kriging. The main difference between the methods is in the technique used to estimate the averages. When the average altitude of a river is unknown, ordinary kriging or universal kriging should be applied instead of simple kriging. In this study, the data for the open channel was used to create the bathymetric contour lines.

Generally, ordinary kriging should meet the best linear unbiased estimate and the following linear condition:

$$Z_0^* = \sum_{i=1}^{n} \lambda_{0i} Z_i \quad (i = 1, 2, \ldots, n) \tag{1}$$

It should also meet the following unbiased condition:

$$E(Z_0^*) = E(Z_o) \tag{2}$$

Therefore, the factor resolution can be obtained through optimization and is given as follows:

$$\min \left\{ Var(Z^* - Z_0) = E\left[(Z_0 - Z^*)^2 \right] \right\} \tag{3}$$

From Eqs. (1) and (2), the following equation is obtained:

$$\sum_{i=1}^{n} \lambda_{0i} = 1 \tag{4}$$

By assuming $E(Z(x)) = E(X(x + h)) = const$, applying the standard Lagrangian, and using Eqs. (1) and (3), the following equation can be obtained:

$$
\begin{aligned}
L &= Var\left[Z^*(x_0) - Z(x_0) \right] - 2m\left(\sum_{i=1}^{n} \lambda_{0i} - 1 \right) \\
&= E\left[Z^*(x_0) - Z(x_0) \right]^2 - 2m\left(\sum_{i=1}^{n} \lambda_{0i} - 1 \right) \\
&= -\sum_{i=1}^{n}\sum_{j=1}^{n} \lambda_{0i}\lambda_{0j}\gamma(x_i - x_j) + 2\sum_{i=1}^{n} \lambda_{0i}\gamma(x_i - x_j) - 2m\left(\sum_{i=1}^{n} \lambda_{0i} - 1 \right)
\end{aligned}
\tag{5}
$$

By differentiating λ and m in Eq. (5), we obtain the following:

$$\frac{\partial L}{\partial \lambda} = 0 \tag{6}$$

$$\frac{\partial L}{\partial m} = 0 \tag{7}$$

Therefore, an ordinary kriging system can be expressed in an array as follows:

$$
\begin{bmatrix}
\gamma_{11} & \gamma_{12} & \cdots & \gamma_{1n} & 1 \\
\gamma_{21} & \gamma_{22} & \cdots & \gamma_{2n} & 1 \\
\vdots & \vdots & & \vdots & \vdots \\
\gamma_{n1} & \gamma_{n2} & \cdots & \gamma_{nn} & 1 \\
1 & 1 & \cdots & 1 & 0
\end{bmatrix}
\begin{bmatrix}
\lambda_1 \\
\lambda_2 \\
\vdots \\
\lambda_n \\
\mu
\end{bmatrix}
=
\begin{bmatrix}
\gamma_{10} \\
\gamma_{20} \\
\vdots \\
\gamma_{n0} \\
1
\end{bmatrix}
\tag{8}
$$

In this array,

$$\gamma_{ij} = \gamma\left[\left| x_i - x_j \right| \right] = \frac{1}{2} E\left\{ \left[Z(x_i) - Z(x_j) \right]^2 \right\} \tag{9}$$

The ordinary kriging variables are given as follows:

$$\sigma_{OK}^2 = Var\left[Z_0^* - Z_0 \right] = \mu + \sum_{i=1}^{n} \lambda_{0i}\gamma(x_i - x_0) \tag{10}$$

Eq. (9) is a semivariogram, which indicates changes between variables in a space. These changes are only related to the distance ($\left| x_i - x_j \right|$). Therefore, a semivariogram increases as the distance between two random variables increases and becomes constant when the distance increases to a certain degree. This represents the independence between two variables. In this study, the applied random variables were selected as the index mode, calculated by Eq. (11)
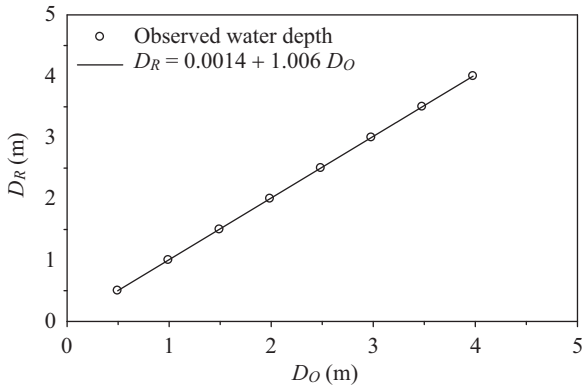
Fig. 6. **Calibration of the pressure sensor**

Fig. 7. **Map of the survey route.**

$$\gamma\left(d\right) = \sigma^2 \left[1 - \exp\left(-\frac{d}{L}\right)\right] \tag{11}$$

IV. RESULTS AND DISCUSSION

In this study, a recording manometer with a built-in data log and without autotransmission function was used to constantly record the pressure. Therefore, the readings at the measurement points could only be read after completing the measurements. The measurement range for the pressure gauges was 0-4 m in depth with an error of 0.3 cm. The pressure measured by the pressure gauge was the absolute pressure. Another pressure gauge was used to measure the atmospheric pressure, which was deducted from the pressure measured by the pressure gauge in the water to obtain the water pressure. The relationship between the pressure and depth is as follows:

$$p = \rho g h \tag{12}$$

where p is the relative pressure (Pa), ρ is the water density (the density of fresh water is 1000 kg/m^3 and that of salt water is 1030 kg/m^3), and g is the gravitational acceleration. Lab calibrations were performed before the measurements to assure the data quality. The results of the calibrated water gauge are displayed in Fig. 6. The horizontal axis represents the depth measured with the water gauge, and the vertical axis represents the actual depth. The results exhibited a linear relationship, confirming the accuracy of the measured water depth.

Measuring the control point is essential before measuring the depth. In this study, a GPS was used to determine the Cartesian coordinates for the location of the total station. Moreover, the benchmark from the Water Resources Agency was used to determine the altitude of the location of the total station by direct observation. The coordinates and altitude of the water surface could be observed from the reflective prism on the surface of the buoys at the total station, and they were obtained by averaging multiple measurements. The altitude of the channel bottom was obtained by subtracting the water depth from the surface altitude,
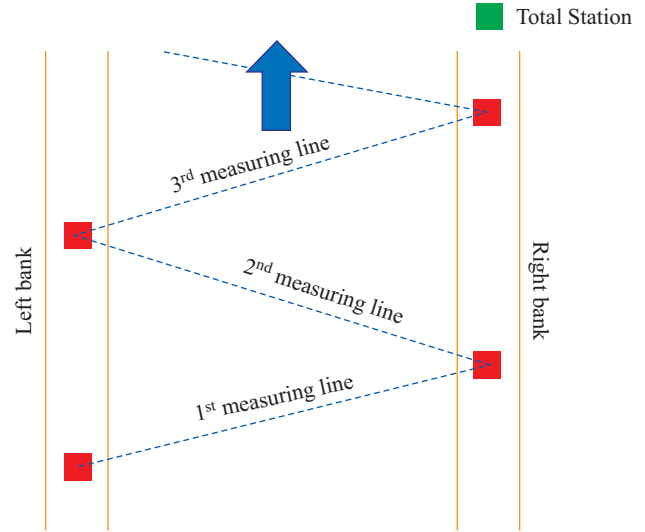
which enabled the altitude and coordinates at the measurement point to be accurately obtained.

To obtain the coordinates and altitude of the channel bed at various locations along the tidal stream, the pressure gauges were moved from one location to another. Cranes were used to transfer the pressure gauges to the specified measurement points. In this study, the bathymetry was measured from the discharge to the end of the sea embankment, which was a length of 142 m. A pile point was set every 10 m along both riverbanks. The starting point was 0 m and the ending point was 100 m. Thus, 11 points were used for mounting the crane. At the right riverbank, the measurement started from 0 m and ended at 150 m. A pile point was set every 15 m. Thus, 11 points were used to mount the crane on the right bank. Pile points along the right and left bank were connected to form a measurement line with eight measurement points. Because the river width was 40-50 m, the space between two measurement points was approximately 5-6 m. A suitable measurement density should be used. After completing the measurement along the measurement line, the crane moved alternatively to the pile points along the right and left banks. After the measurement along the first measurement line was completed, the pile point on the right bank was fixed and the pile point on the left bank was moved to the next measurement point for measurement on the second measurement line. After the measurement along the second measurement line was completed, the pile point on the left bank was fixed and the pile point on the right bank was moved to the next measurement point for measurement on the third measurement line. The measurements were performed in a zigzag manner, as displayed in Fig. 7. As displayed in Fig. 8, measurement was performed at 179 points along the channel, which was a high measurement density. The kriging method was used for the best linear unbiased prediction of the intermediate water depths between the observed points. Fig. 9 displays a topographic map interpolated using the kriging method for the altitudes and co-
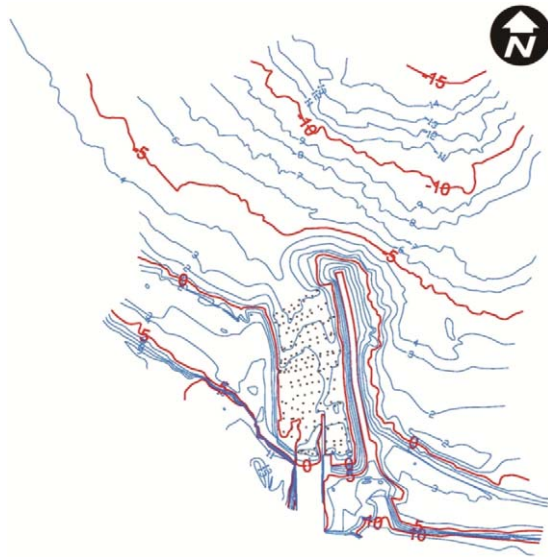
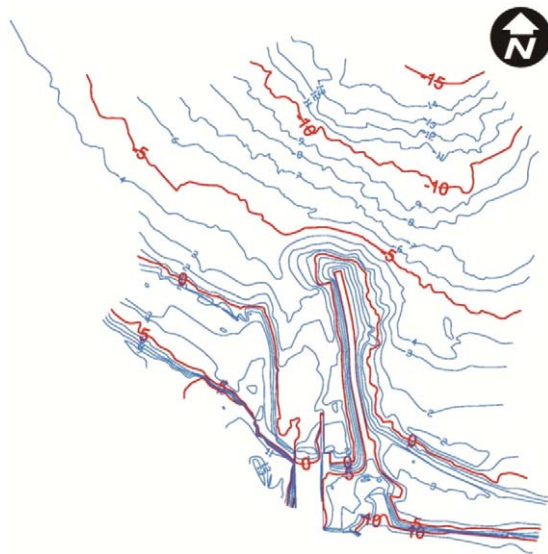**Fig. 8. Water depth measurement locations.**

Fig. 9. Orography of the open channel in the tidal flat.

ordinates from 179 points. The channel topography was accurately obtained from these highly dense measurements. The results demonstrated the suitability of this measuring system and calculation method for depth measurements of the studied channel.

V. CONCLUSIONS

Certain terrain and flow conditions prevent the application of common bathymetry measurement methods. Therefore, a simple and reliable system was developed to measure the bathymetry of the study area. Understanding the topography of an open channel is essential for managing water resources. However, suitable techniques and instruments should be used depending on the river stream environment and flow conditions.

The proposed system had some limitations. The first was its unsuitability for open channels with a large width and high velocity. If the channel cross-section is particularly wide, then setting up and operating the system becomes extremely difficult. A strong current causes the sounding weight to drift from the desired location. The measurement equipment was transferred by cranes to the measurement points. Subsequently, the total station was used to measure the altitude and coordinates at the measurement points, and pressure gauges were used to accurately measure the depth. Thus, the bottom altitude and coordinates were calculated. Kriging interpolation was used to interpolate the measured topographic data for obtaining the channel topography of the tidal river. The advantages of this measurement system include its ease of use, low cost, and accuracy. Primarily, it allows measuring the topography of a tidal river, which was previously impossible.

REFERENCES

Chen, Y.-C., S.-P. Kao and H.-W. Chiang (2013). Defining and estuary using the Hilbert-Huang transform. Hydrolog. Sci. J. 58, 841-853.

Garrison, T. (2007). Oceanography: An Invitation to Marine Science. Thomson, Belmont, CA.

Guenther, G. C., A. G. Cunningham, P. E. LaRocque and D. J. Reid (2000). Meeting the accuracy challenge in airborne lidar bathymetry. In: Reuter, R. (Ed.). Proceedings of EARSeL-SIG Workshop LiDAR No. 1, Dresden, Germany.

Gupta, S.D., I. M. Shahinur, A. A. Haque, A. Ruhul and S. Majumder (2012). Design and implementation of water depth measurement and object detection model using ultrasonic signal system. International Journal of Engineering Research and Development 4, 62-69.

Hughes Clarke, J. E., L. A. Mayer and D. E. Wells (1996). Shallow-water imaging multibeam sonars: A new tool for investigating seafloor processes in the coastal zone and on the continental shelf. Mar. Geophys. Res. 18, 607-629.

Kvale, E. P. (2006). The origin of neap-spring tidal cycles. Mar. Geol. 235, 5-18.

Muirhead, K, and A. P. Cracknell (1986). Airborne lidar bathymetry. Int. J. Remote Sens. 7, 597-614.

Pachecoa. A., O. Ferreira, J. J. Williams, E. Garel, A. Vila-Concejo and J. A. Dias (2010). Hydrodynamics and equilibrium of a multiple-inlet system. Mar. Geol. 274, 32-42.

Pe'eri, S., L.V. Morgan, W. Philpot and A. A. Armstrong (2011). Land-Water Interface Resolved from Airborne LIDAR Bathymetry (ALB) Waveforms. J. Coastal Res. 62, 75-85.

Rantz, S. E. (1982) Measurement and Computation of Streamflow: Vol. 1. Measurement of Stage and Discharge. United States Government Printing Office, Washington, DC.

Rodriguez-Iturbe, I., M. G. Sanabria and R. L. Bras (1982). A geomorphoclimatic theory of the instantaneous unit hydrograph. Water Resour. Res. 18, 877-886.

Schwiderski, E. W. (1980). On charting global ocean tides. Rev. Geophy. 18, 243-268.

US Army Corps of Engineers (2004). Hydrographic Surveying. Department of the Army US Army Corps of Engineers, Washington, DC.

Wang, C. K. and W. D. Philpot (2007). Using airborne bathymetric LIDAR to detect bottom type variation in shallow waters. Remote Sens. Environ. 106, 123-135.